Solar Energy 193 (2019) 986–991

Contents lists available at ScienceDirect

Solar Energy

journal homepage: www.elsevier.com/locate/solener

Superficial composition engineering for oxide nanoparticles derived $Cu_2ZnSn(S, Se)_4$ solar cells by a three-step annealing process

Huiling Cai[a,b], Liquan Yao[a], Yingsen Xia[a], Chunyan Dao[a], Jianmin Li[c,*], Limei Lin[a,b], Zhiping Huang[a,b], Guilin Chen[a,b,*]

[a] Fujian Provincial Key Laboratory of Quantum Manipulation and New Energy Materials, College of Physics and Energy, Fujian Normal University, Fuzhou 350007, China
[b] Fujian Provincial Collaborative Innovation Center for Optoelectronic Semiconductors and Efficient Devices, Xiamen 361005, China
[c] Department of Physics, The Chinese University of Hong Kong, Shatin, Hong Kong

ARTICLE INFO

Keywords:
$Cu_2ZnSn(S, Se)_4$
Thin films
Solar energy materials
Post-sulfurization

ABSTRACT

In this work, a three-step (sulfurization-selenization-sulfurization) annealing process was designed to optimize the surface constitution of $Cu_2ZnSn(S, Se)_4$ (CZTSSe) thin films, which was prepared by oxide nanoparticles-based approach. The devices with the Mo/CZTSSe/CdS/ZnMgO/ZnO:Al/Al structure were fabricated and their performances were studied. The additional post-sulfurization with low toxicity sulfur powder has negligible impact on the structure, morphology and composition of CZTSSe bulk, however, it improves open circuit voltage of device significantly. The open circuit voltage can be increased significantly from 408 mV (without surface sulfurization) to 497 mV (with surface sulfurization). This is benefited from the increase of surficial sulfur content and the broadening of the surface band-gap of the CZTSSe thin film. The result is confirmed by X-ray photoelectron spectroscopy analysis. Such a crucial three-step annealing process promotes the power conversion efficiency from 4.71% (2-step) to 6.37% (3-step), which is the champion efficiency of oxide precursor derived CZTSSe solar cell.

1. Introduction

$Cu_2ZnSn(S, Se)_4$ (CZTSSe) is considered as a promising material for thin film solar cells since it is composed of low-toxic and earth-abundant elements (Kim et al., 2018). Moreover, CZTSSe has a large absorption coefficient ($> 10^4\ cm^{-1}$) and a tunable band-gap (1.0–1.5 eV) (Franckevičius et al., 2019). The record power conversion efficiency (PCE) of 12.6% (Wang et al., 2014) was obtained via a hydrazine-based process, but it is not a safe way to be popularized due to the use of toxic reagent. So many eco-friendly and non-vacuum methods are widely developed for CZTSSe thin films. Specially, the nanoparticles (NP)-based approach is deemed to be a candidate for CZTSSe because of the high material utilization. By comparing with other NP precursors such as quaternary, binary compound and metal alloy, the synthesis of oxide NP is facile, low-cost and air-insensitive, which has been successfully applied in Cu(In, Ga)Se_2 (CIGS) and CZTSSe (Chen et al., 2017; Kapur et al., 2003). A stable oxide precursor can control the growth of chalcogenide thin film without component losses. Besides, compact film can be easily obtained through volume expansion caused by the conversion of oxide NP into chalcogen. So the oxide NP-based approach was considered as one of promising coating techniques for chalcogenide thin films. Such an excellent oxide NP derived approach has achieved a PCE of 13.6% in CIGS device, which has also been industrialized by ISET (Kapur et al., 2003). However, the performance of CZTSSe device is still hindered by the low open circuit voltage (V_{oc}) when compared with CIGS. The V_{oc} deficit is one of the key factors limiting CZTSSe solar cells so far (Wanda et al., 2019). Several reasons for V_{oc} restrictions have been proposed: (1) band-gap fluctuations due to compositional nonuniformities or potential fluctuations rising from high concentration of charged defects (Xu et al., 2018). (2) Undesirable band alignment at the PN junction (Sun et al., 2016). (3) High recombination rate due to the presence of secondary phase and defect states in the absorber or its interface (Platzer-Bjorkman et al., 2015).

To resolve the V_{oc} deficit for higher PCE of CZTSSe devices, many means have been developed. Among them, the sulfur element doping treatment has been proven to effectively engineer the band-gap and then improve the V_{oc} of the CZTSSe devices (Hwang et al., 2017). For example, Jun He et al. have prepared CZTSSe powders with different S/Se ratios, in which the absorption spectra shows that the band-gap of CZTSSe solid solution increases almost linearly with the increase in the

* Corresponding authors at: Fujian Provincial Key Laboratory of Quantum Manipulation and New Energy Materials, College of Physics and Energy, Fujian Normal University, Fuzhou 350007, China (G. Chen).
E-mail addresses: b142916@cuhk.edu.hk (J. Li), glchen@fjnu.edu.cn (G. Chen).

https://doi.org/10.1016/j.solener.2019.10.026
Received 7 July 2019; Received in revised form 2 September 2019; Accepted 14 October 2019

S content (He et al. (2012)). CZTSSe absorber layers with various S/(S + Se) ratios at the surface and in the bulk have also been synthesized to investigate the effect of the S/(S + Se) ratios on the performance of the CZTSSe device. Kim et al. have obtained band-gap graded CZTSSe films by heat treatment under a non-uniform vapor condition of S and Se (Kim et al., 2019). Conventionally the sulphur gradient of CZTSSe films should be accompanied by a band-gap gradient after sequential sulfurization and selenization, meaning that the band-gap at the PN-junction should be lower than the band-gap at the back of the absorber (Neuwirth et al., 2018). To widen the surface band-gap of CZTSSe films as well as enhance V_{oc} of device, the surficial composition was optimized by many groups. For instance, Hwang et al. substitutes S for Se in the near-surface region of absorber layer to get band-gap front-graded CZTSSe thin films (Hwang et al., 2017). The devices exhibit high V_{oc}, low V_{oc} deficit, and less loss of J_{sc}, which are attributed to the surface band-gap widening and passivation of deep recombination centers within the space charge region of the device. Cai et al. have also revealed that V_{oc} can be significantly enhanced from 312 mV to 400 mV by introducing H_2S gas during the cooling stage of selenization, which can be attributed to the reduction of interface recombination and the increase of surface band-gap (Cai et al., 2017). But the explosive and highly toxic H_2S gas was required during annealing. Similarly, Wang et al. prepared CZTSSe by DC-magnetron sputtering with a single Cu-Zn-Sn target, followed by a H_2S-sulfurization-after H_2Se-selenization (SAS) process. Surface sulfurization was implemented to modify the front surface, which significantly reduced the surface defects (Wang et al., 2017a,b). But further large-scale production could be restricted by the toxicity and flammability of H_2S gas.

In our previous work, we have prepared CZTS using low-cost oxide NP method. A two-temperatures zone tube furnace was used to study the effect of sulfur vapor pressure on the morphology and crystalline of CZTS thin films. The PCE of the device based on the sulfurized CZTS thin film was 2.59% (Wang et al., 2017a,b). Post-selenization was further implemented to improve the crystallinity and reduce the defect concentration of the CZTS film, thereby improving the film quality. We have obtained CZTSSe devices with a PCE of 4.4% by oxide NP method (Chen et al., 2017). However, the sequential sulfurization and selenization will narrow band-gap of CZTSSe surface (Todorov et al., 2010), which lowers the low V_{oc}. Therefore, a three-step annealing process was applied to obtain oxide NP derived CZTSSe thin film in this work, in which the post-sulfurization (third step) under sulfur vapor was used to widen the band-gap of front surface and so as to improve the V_{oc} of the device.

2. Experimental

Oxide precursor thin films were prepared by depositing oxide ink on a 1-μm-thick molybdenum (Mo)-coated soda-lime glass (SLG) by doctor blade process. Such ink could be obtained as follow: the metal salts (Cu $(NO_3)_2{\cdot}3H_2O$ (99.99%, Sinopharm Chemical Reagent Co., Ltd.), Zn $(NO_3)_2{\cdot}6H_2O$ (99.99%, Sinopharm Chemical Reagent Co., Ltd.), SnC_2O_4 (98.0%, Shanghai Aladdin Biochemical Technology Co., Ltd.) and NH_4HCO_3 (99.0%, Sinopharm Chemical Reagent Co., Ltd.)) were first mixed at a certain molar ratio and ground uniformly with an agate mortar, and then sintered at 380 °C for 30 min to obtain oxide powders. Oxide powders were then uniformly dispersed in alcohol using a high-energy ball mill to form oxide ink. More details about the preparation of oxide precursor can refer to our previous report (Chen et al., 2015). As shown in Fig. 1, the oxide NP derived CZTSSe thin films were prepared by a three-step annealing process. In brief, the precursor films were first sulfurized at 580 °C for 30 min (base $\sim 10^{-1}$ Pa) with 0.02 g sulfur powder (S, 99.9%), which were sequentially selenized under 550 °C for 20 min (base $\sim 10^{-1}$ Pa) with 0.015 g selenium powder (Se, 99.9%). Finally, the surface of the obtained CZTSSe thin films were further modified by S vapor under flowing Ar gas (50 sccm) at 450 °C for 3 min to replace part of the surface selenium by sulfur. The heating ramp rate

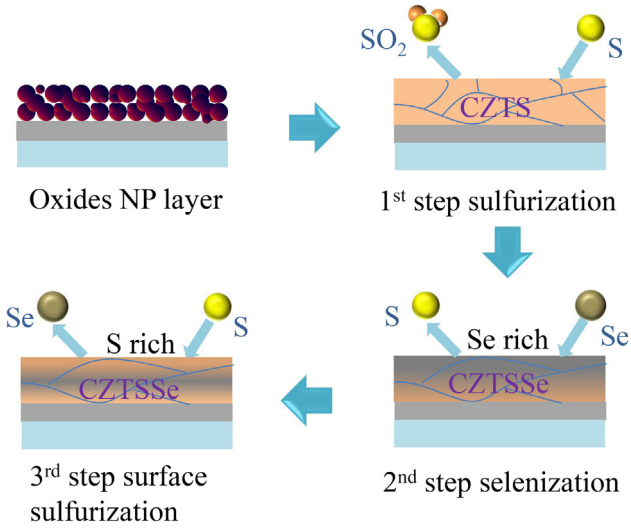

Fig. 1. Schematic diagram of 3-step annealing process for CZTSSe thin films.

of annealing process was fixed at 50 K/min. After the CZTSSe thin films were deposited on molybdenum coated glass substrate, photovoltaic devices were completed by the chemical bath deposition of CdS (~70 nm), sputtering of ZnMgO (50 nm), ZnO:Al (400 nm) and electron-beam evaporation of aluminum grids. Devices were then scribed into 0.5 cm^2.

The structure of the thin film was studied by X-ray diffraction (XRD) with Cu Kα irradiation (λ = 1.54178 Å) and Raman measurement (LABRAM-HR) with excitation wavelength of 532 nm. The morphology of the film was characterized by field emission scanning electron microscope (SEM, JSM-6700F). The composition of the film was measured by Energy Dispersive X-ray Spectroscopy (EDX). The optical absorption spectrum was recorded on a UV–vis-365-type spectrophotometer in a range of 400–1600 nm. The X-ray photoelectron spectroscopy (XPS) spectra were carried out on Thermo Fisher Scientific K-Alpha spectrometer using an Al K alph monochromatized source under a 10^{-8} Pa residual pressure. The current density-voltage (*J*-V) curves were tested by Keithley 4200-SCS with an AAA SAN-EI Electric solar simulator under AM 1.5, 25 °C.

3. Results and discussions

The typical tope-view and cross-section morphologies of CZTSSe thin films prepared under 2-step and 3-step annealing process are shown in Fig. 2(a, c) and (b, d), respectively. It is obvious that both of the front surfaces are uniform and smooth. The small and bright particles are likely to be ZnS as the samples are all with Zn-rich component. The thickness of the absorber film is approximately 1.5 μm. In addition, we can see that the 2-step annealed film is not completely dense. And there are still some holes, although very few. These holes provide sufficient space for stress relief so that the film does not crack when large atomic selenium replaces small sulfur atomic during the third step. It is notable that there is no significant difference between the 2-step and 3-step treated samples, which indicates that the surface sulfurization did not bring obvious morphological changes to CZTSSe layers.

The crystal structure of the 2-step and 3-step treated films were detected by XRD (Fig. 3). Both the relevant XRD patterns possess sharp and strong diffraction peaks, which can be assigned to the (1 1 2), (2 2 0) and (3 1 2) planes of Kesterite type CZTSSe. Using the diffraction pattern from the underlying Mo substrate as a 2θ calibration reference, the peak from (1 1 2) plane of 3-step treated film at 27.6° slightly shifts to larger degree when compared with that of 2-step processed film. This result can be attributed to the shrink of unit cell volume at the surface whereby the replacement of bigger atom by smaller atom. (Hassanien

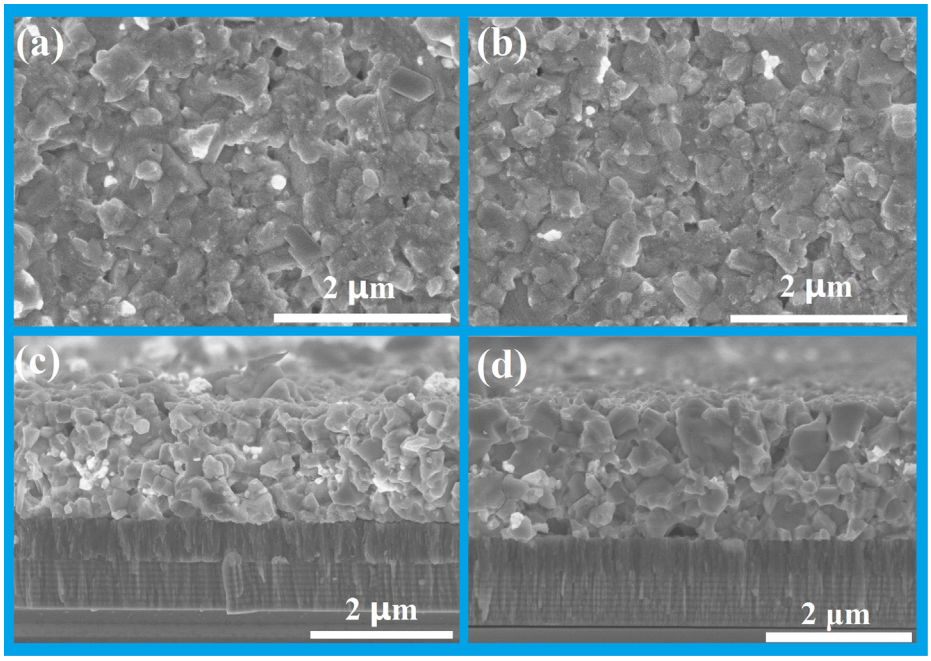

Fig. 2. SEM images of CZTSSe thin films prepared by 2-step (a, b) and 3-step (c, d) annealing process.

et al., 2018; Dimitrievska et al., 2016). Consequently, it is rational to assume the third step (surface sulfurization) can replace some of the Se atoms with S atoms and slightly enlarge the sulfur content of CZTSSe thin film. Meanwhile, the band-gap of CZTSSe increases monotonically with the increase in the sulfur content (Ferhati and Djeffal, 2018). This process is expected to widen the surface band-gap of CZTSSe thin film and increase the V_{oc} of the device further (Barkhouse et al., 2012).

Raman spectroscopy was used to further analyze the obtained CZTSSe thin films. The Raman spectrums of 2-step and 3-step treated films are shown in Fig. 4(a) and (b), respectively. The signals from different depths of the film were detected with various laser intensities (5%, 10%, 25%, 50% and 100%). The peaks at 204 cm^{-1} and 325 cm^{-1} are corresponding to CZTSe and CZTS respectively (Salomé et al., 2012). While the peak at 402 cm^{-1}, which can be assigned to MoS_2, appeared once a higher laser intensity was introduced (Barkhouse et al., 2012). The intensity ratio of Raman main mode (CZTSe/CZTS) versus laser power is shown in Fig. 4(c). It reveals that the S/Se ratio of 3-step treated film is slightly higher than that of 2-step treated film, which is consistent with the XRD result (Fig. 3). Meanwhile, the compositions of 2-step and 3-step treated CZTSSe thin films measured by EDX are shown in Table 1. The ratios of Cu/(Zn + Se) and Zn/Sn are about 0.84–0.87 and 1.36–1.40, respectively. It is generally believed that such a Cu-poor and Zn-rich component will increase the P-type characteristics of CZTSSe. In fact, the Cu-poor component promotes the formation of Cu vacancies, which acts as shallow acceptors in the CZTS film. Under Zn-rich conditions, the substitution of Cu for Zn vacancies can be reduced, which notably reduces the deep acceptors (Haddout et al., 2019). Such Cu-poor and Zn-rich component generally leads to higher efficiency as a Zn-rich content can suppress the formation of shallow acceptors (Cu_{Zn}) (Chen et al., 2010; Shin et al., 2017). Besides, the S/Se ratio of the 2-step treated film (0.65) and 3-step treated film (0.66) exhibit only slight increasement after post sulfurization, which again agrees well with the results of XRD and Raman.

The ban-gap of absorber film is an important factor for device performance. So the transmittance spectrum was recorded in the range of 300–1600 nm, as shown in Fig. 5. Beginning at about 1100 nm, the

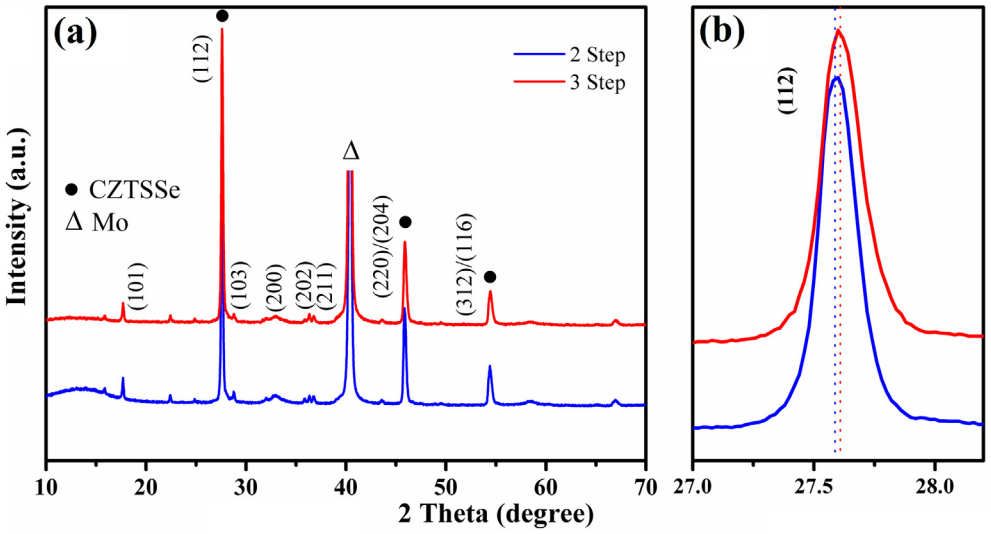

Fig. 3. (a) XRD patterns of CZTSSe thin films prepared by 2-step and 3-step annealing process, (b) enlarged peak of (1 1 2).

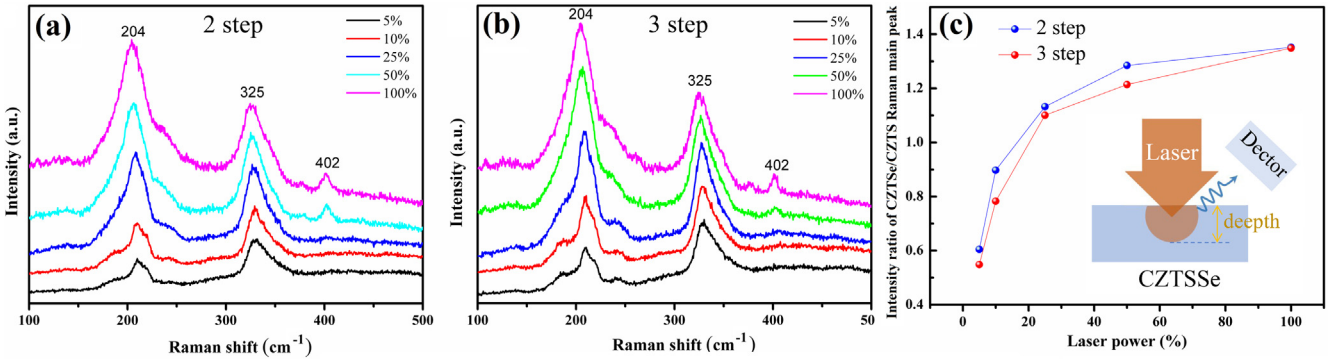

Fig. 4. Raman spectrums of CZTSSe thin films prepared by (a) 2-step and (b) 3-step annealing process, (c) intensity ratios of Raman main mode (CZTSe/CZTS).

Table 1
Elemental composition of CZTSSe thin films based on 2-step and 3-step annealing.

Sample	Cu/(Zn + Sn)	Zn/Sn	S/Se
2-Step	0.87	1.36	0.65
3-Step	0.84	1.40	0.66

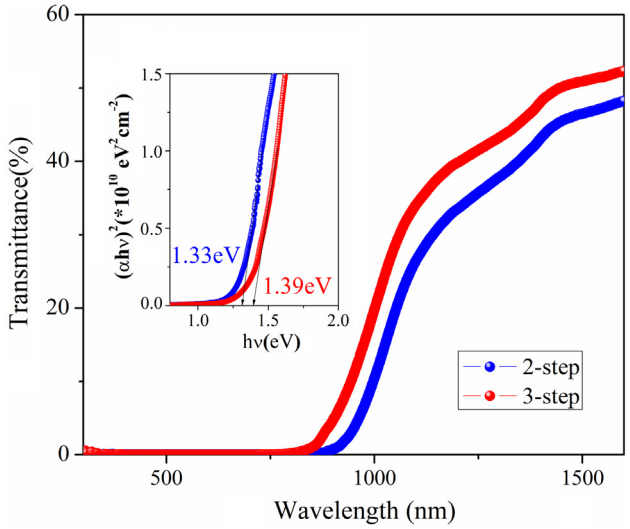

Fig. 5. The transmission spectrum of 2-step and 3-step derived CZTSSe thin films. Inset: Tauc plot of $(ah\nu)^2$ vs hν for the value of band-gap estimation.

transmittance of 2-step and 3-step treated CZTSSe thin films reduce steeply and decrease to almost zero at wavelength shorter than 910 nm and 845 nm respectively. It indicated that both 2-step and 3-step treated CZTSSe thin films possess high absorbance in the visible region. To further study the influence of post-sulfurization on optical properties of CZTSSe thin films, the band-gap was determined by the plot of $(\alpha h\upsilon)^2$ vs hυ (Hassanien and Sharma, 2019; Hassanien and Akl, 2015) in the inset of Fig. 5. The band-gap values were calculated to be 1.33 and 1.39 eV for CZTSSe thin films prepared by 2-step and 3-step annealing, respectively. It can be clearly seen that the transitory sulfurization only widens the band-gap of CZTSSe bulk by 0.06 eV, attributing to the trace S doping. In brief, the mild post-sulfurization (3rd step) has negligible impact on the structure, morphology, composition and band-gap of CZTSSe bulk.

The *J*-V curves of the devices based on 2-step and 3-step treated films are shown in Fig. 6. The performance metrics of device are extracted in Table 2. Obviously, the V_{oc}, J_{sc}, FF and PCE of the device based on 3-step treated film are 497 mV, 23.4 mA/cm^2, 54.7%, and 6.37%, respectively. To the best of our knowledge, this is the champion PCE of oxide NP derived CZTSSe devices. It is not difficult to work out the increase of V_{oc} is about 22% (408–497 mV) and PCE is about 35% (4.71–6.37%) with an almost loss-free J_{sc} (decreases about 0.09%). Previous serial analyses have verified that the short post-sulfurization process has weak influence on CZTSSe bulk. To understand the enhancement of device performance, the evolution of surficial composition was examined by XPS. Fig. 7 shows the XPS spectra of Cu 2p, Zn 2p, Sn 3d, Se 3p & S 2p, and Se 3d in CZTSSe thin film. The Cu, Zn and Sn core levels of 2-step and 3-step derived CZTSSe are similar. For examples, the peak of Cu 2p is split into Cu $2p_{3/2}$ and Cu $2p_{1/2}$ with a split orbit of 19.8 eV, demonstrating the exits of Cu (I). The peaks of Zn $2p_{3/2}$ and Zn $2p_{1/2}$ appear at binding energy (BE) of 1021.4 eV and 1044.5 eV, which belong to Zn (II). The Sn $M_4N_{45}N_{45}$ Auger peak at BE = 1051.9 eV can be observed on the high energy side of the Zn 2p core level spectra. The Sn (IV) shows doublet peaks at 486.1 eV ($2d_{5/2}$) and 494.8 eV ($2d_{3/2}$) with its characteristic peak separation of 8.7 eV. The Zn $L_3M_{45}M_{45}$ Auger peak at BE = 496.7 eV can also be observed on the high energy side of the Sn 3d core level spectrum. All the characteristic peaks of XPS confirm the formation of CZTSSe with 2-step or 3-step annealing. The S 2p and Se 3p core level spectrum were closely inspected to reveal the S/Se component variation in Fig. 7(d, i). Both S ($2p_{1/2}$, $2p_{3/2}$) and Se ($3p_{1/2}$, $3p_{3/2}$) were observed in 2-step derived CZTSSe thin films, which confirmed the coexistence of S and Se on the surface. However, the Se ($3p_{1/2}$, $3p_{3/2}$) fade away after intruding 3rd step, while the intensity of S ($2p_{1/2}$, $2p_{3/2}$) peaks are enhanced, which manifests the superficial Se atom is substituted by S. This is also confirmed by the Se 3d core level spectrum (Fig. 7(e, j)). When the post-sulfurization was carried out, the peaks of Se 3d were weakened. Using the integral area of S 2p and Se 3d peaks, the S/Se ratios are calculated to be 3.0 and 5.5 for surficial composition of 2-step and 3-step treated CZTSSe, demonstrating the CZTSSe thin film becomes S richer after post-sulfurization. Those results in line with the EDX, XRD and Raman dates again. In short, the post-sulfurization can affect the superficial composition of S/Se in CZTSSe significantly.

In this work, the superficial band-gap of 2-step based CZTSSe thin film was narrowed when exposed under Se vapor during the 2nd selenization, as demonstrated in Fig. 6(b). Once the illumination excites electron-hole pairs, such a gradient band-gap favors the electron transport toward CdS buffer layer. However, the small band-gap forms a junction with CdS at the interface will pull down the V_{oc}. For the highly efficient CIGS thin films solar cell, a 'V' shaped band-gap was always designed to reduce recombination and enhanced separation of photo-generated carriers (Niu et al., 2014). The above XPS analysis has indicated that the post-sulfurization can increase the sulfur content of CZTSSe surface notably, in which band-gap grading was realized within the depletion region (Fig. 6(b)). It is also noted that the large superficial band-gap can improve the V_{oc}. On account of the unconspicuous variation of band-gap of CZTSSe bulk after post-sulfurization, the V_{oc} deficit can be decreased from 922 mV to 893 mV significantly. On the other hand, the electron can be wiped out of the depletion region by

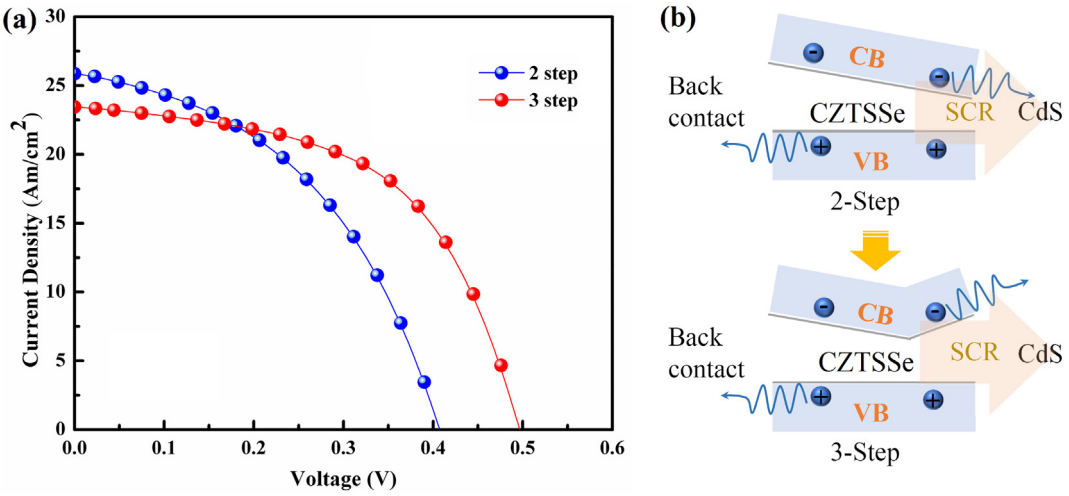

Fig. 6. *J*-V curves of CZTSSe devices prepared by 2-step and 3-step annealing process.

Table 2
Performance metrics of CZTSSe solar cells based on 2-step and 3-step annealing.

CZTSSe	J_{sc} (mA/cm^2)	V_{oc} (mV)	FF (%)	PCE (%)	E_g of bulk (eV)	V_{oc} deficit (mV)
2-Step	25.8	408	44.7	4.71	1.39	922
3-Step	23.4	497	54.7	6.37	1.33	893

built-in internal electric field, and then collected by the cathode. So the 'V' shaped band-gap of the CZTSSe layer constructed in this work can improve the V_{oc} with an almost loss-free J_{sc} compared to the uniform band-gap CZTSSe (Yang et al., 2016), which is similar to the case of CIGS (Dullweber et al., 2001; Gloeckler and Sites, 2005). Therefore the satisfied performance of 3-step processed device can be attributed to the formation of induced surface constitution after post-sulfurization, although the post-sulfurization degree for CZTSSe bulk is very weak.

Copper based ternary and quaternary semiconductor are of great interest for the fabrication of low-cost photovoltaics. To data, many methods have been developed for preparation of the relevant thin films. Among them, oxide precursor route is potential for mass production due to the low-cost, non-toxic raw materials and facile synthesis process. Meanwhile, this method can resist the possible element loss during post-annealing because of the relative high stability of oxides, which can control the reaction pathway well. Herein, we briefly review the state-of-the-art solar cell development of copper-based ternary and quaternary absorber by oxides-based routes, as shown in Table 3. For example, the oxides NP-derived CIGS has been successfully manufactured by ISET, which have achieved efficiency of 13.8% (Kapur et al., 2003). To eliminate the use of the scarcity of In, Ga, other absorbers including CZTSSe and Cu_2SnS_3 (CTS) etc. have also been developed using oxides precursor. The oxides-derived CTS solar cell was scarcely reported with very poor performance, while CZTSSe solar cell have been studied by several group. For instant, Fukano et al. have obtained 6% efficiency Cu_2ZnSnS_4 solar cells using oxide precursors by CVD (Washio et al., 2012). Jin et al. have fabricated 4.94% efficiency CZTSSe solar cells using oxide precursors by PLD (Jin et al., 2016). Zhu and Liu group have achieved CZTS thin films with PCE of 1.6% and 1.22% respectively, which uses oxides NP precursor synthesized by combustion and precipitation (Jin et al., 2016; Tang et al., 2013). Our group firstly introduced the oxides NP precursor into CZTS thin films in 2015, but the relevant device only exhibited efficiency of 1.47%. In this work, the post-sulfurization improves the efficiency of oxides-derived CZTSSe thin films solar cell to 6.13%. Although the performance of oxides-based CZTSSe solar cell is still lower than that of toxic hydrazine

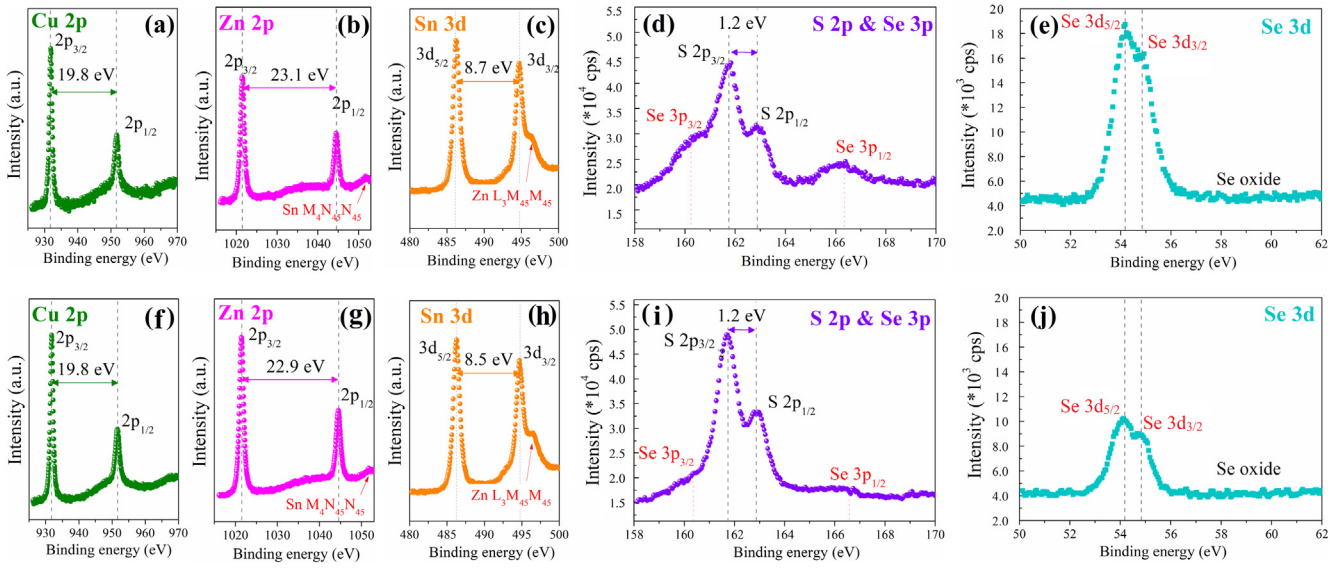

Fig. 7. XPS spectra of (a–e) and (f–i): Cu 2p, Zn 2p, Sn 3d, Se3p & S2p, and Se 3d core levels of 2-step and 3-step derived CZTSSe thin films respectively.

Table 3
Oxides precursor-derived Cu-based absorber for solar cell.

Materials		Preparation of oxides	V_{oc} (mV)	J_{sc} (mA/cm^2)	FF (%)	PCE (%)	Group	Ref.
CIGS		Precipitation	520	37.3	71	13.6	ISET	Kapur et al. (2003)
CZTS(Se)	CZTS	CVD	654	15.5	52	5.26	Fukano	Washio et al. (2012)
	CZTSSe	PLD	684	16.82	42.8	4.94	Zhu	Jin et al. (2016)
	CZTS	Precipitation	320	9.28	41	1.22	Liu	Tang et al. (2013)
	CZTS	Combustion	505	10.5	30.3	1.60	Zhu	Jin et al. (2016)
	CZTSSe	Solvent-free	497	23.4	54.7	6.37	Chen	This work
CTS		Solvent-free	300	2.3	22.6	0.16	Chen	Wang et al. (2018)

method, the further optimization of preparation process is expected to improve the efficiency by using such a green and low cost oxides NP route.

4. Conclusion

In summary, oxide NP-derived CZTSSe thin film has been prepared by a 3-step annealing process. The post sulfurization with sulfur powder was introduced to improve the V_{oc} of the devices by increasing the surficial sulfur content of the CZTSSe films, without obvious variation of structure, morphology and composition. The performance of the CZTSSe device based on 3-step is more superior than that of the 2-step processed device. This change can be attributed to the fact that the surface of the film is modified with sulfur to broaden the surface band-gap and enhance light absorption. Finally, the PCE of CZTSSe solar cell dramatically increases from 4.71% (2-step) to 6.37% (3-step), which is the highest efficiency in oxide precursor derived CZTSSe solar cell.

Acknowledgments

This work was supported by National Natural Science Foundation of China (Grant Nos. 51502037, 61974028), Natural Science Foundation of Fujian Province, China (Grant No. 2015J05096), Fujian Normal University (FNU) Training Program of Innovation and Enterpreneurship for Undergraduates (cxxl-2019135, 2019140, 2019143).

References

Barkhouse, D.A.R., Gunawan, O., Gokmen, T., Todorov, T.K., Mitzi, D.B., 2012. Device characteristics of a 10.1% hydrazine-processed $Cu_2ZnSn(Se, S)_4$ solar cell. Prog. Photovolt.: Res. Appl. 20, 6–11.

Cai, C.H., Wei, S.Y., Huang, W.C., Hsu, C.H., Ho, W.H., Lai, C.H., 2017. Efficiency enhancement of $Cu_2ZnSn(S, Se)_4$ solar cells by S-modified surface layer. Sol. Energy Mater. Sol. Cells 162, 21–29.

Chen, S.Y., Gong, X.G., Walsh, A., Wei, S.H., 2010. Defect physics of the kesterite thin-film solar cell absorber Cu_2ZnSnS_4. Phys. Lett. 96, 021902.

Chen, G.L., Yuan, C.C., Liu, J.W., Huang, Z.G., Chen, S.Y., Liu, W.F., Jiang, G.S., Zhu, C.F., 2015. Fabrication of Cu_2ZnSnS_4 thin films using oxides nanoparticles ink for solar cell. J. Power Sources 276, 145–152.

Chen, G.L., Wang, W.H., Zhang, B.Y., Chen, S.Y., Huang, Z.G., Zhuang, B., 2017. Influence of selenization atmosphere on the $Cu_2ZnSn(S, Se)_4$ thin films and its correlation to the performance of solar cells. Mater. Res. Bull. 94, 164–173.

Dimitrievska, M., Fairbrother, A., Gunder, R., Gurieva, G., Xie, H., Saucedo, E., Perez-Rodrıguez, A., Izquierdo-Roca, V., Schorr, S., 2016. Role of S and Se atoms on the microstructural properties of kesterite $Cu_2ZnSn(S_xSe_{1-x})_4$ thin film solar cells. Phys. Chem. Chem. Phys. 18, 8692–8700.

Dullweber, T., Hanna, G., Rau, U., Schock, H.W., 2001. A new approach to high-efficiency solar cells by band gap grading in $Cu(In, Ga)Se_2$ chalcopyrite semiconductors. Sol. Energy Mater. Sol. Cells 67, 145–150.

Ferhati, H., Djeffal, F., 2018. Graded band-gap engineering for increased efficiency in CZTS solar cells. Opt. Mater. 76, 393–399.

Franckevičius, M., Pakštas, V., Grincienė, G., Kamarauskas, E., Giraitis, R., Nekrasovas, J., Selskis, A., Juškėnas, R., Niaura, G., 2019. Efficiency improvement of superstrate CZTSSe solar cells processed by spray pyrolysis approach. Sol. Energy 185, 283–289.

Gloeckler, M., Sites, J.R., 2005. Band-gap grading in $Cu(In, Ga)Se_2$ solar cells. J. Phys. Chem. Solids 66, 1891–1894.

Haddout, A., Fahoume, M., Qachaou, A., Raidou, A., Lharch, M., Elharfaoui, N., 2019. Influence of composition ratio on the performances of kesterite solar cell with double CZTS layers-A numerical approach. Sol. Energy 189, 491–502.

Hassanien, A.S., Akl, A.A., 2015. Influence of composition on optical and dispersion parameters of thermally evaporated non-crystalline $Cd_{50}S_{50-x}Se_x$ thin films. J. Alloys Compd. 648, 280–290.

Hassanien, A.S., Sharma, I., 2019. Band-gap engineering, conduction and valence band positions of thermally evaporated amorphous $Ge_{15-x}Sb_xSe_{50}Te_{35}$ thin films: Influences of Sb upon some optical characterizations and physical parameters. J. Alloys Compd. 798, 750–763.

Hassanien, A.S., Akl, A.A., Sáaedi, A.H., 2018. Synthesis, Crystallography, microstructure, crystal defects, and morphology of $Bi_xZn_{1-x}O$ nanoparticles prepared by sol-gel technique. CrystEngComm 20, 1716–1730.

He, J., Sun, L., Chen, S.Y., Chen, Y., Yang, P.X., Chu, J.H., 2012. Composition dependence of structure and optical properties of $Cu_2ZnSn(S, Se)_4$ solid solutions: an experimental study. J. Alloys Compd. 511, 129–132.

Hwang, D.K., Ko, B.S., Jeon, D.H., Kang, J.K., Sung, S.J., Yang, K.J., Nam, D., Cho, S., Cheong, H., Kim, D.H., 2017. Single-step sulfo-selenization method for achieving low open circuit voltage deficit with band gap front-graded $Cu_2ZnSn(S, Se)_4$ thin films. Sol. Energy Mater. Sol. Cells 161, 162–169.

Jin, X., Li, J.M., Chen, G.L., Xue, C., Liu, W.F., Zhu, C.F., 2016. Preparation of Cu_2ZnSnS_4-based thin film solar cells by a combustion method. Sol. Energy Mater. Sol. Cells 146, 16–24.

Jin, X., Yuan, C.C., Zhang, L.J., Jiang, G.S., Liu, W.F., Zhu, C.F., 2016. Pulsed laser deposition of $Cu_2ZnSn(S_xSe_{1-x})_4$ thin film solar cells using quaternary oxide target prepared by combustion method. Solar Energy Materials and Solar Cells 155, 216–225.

Kapur, V.K., Bansal, A., Le, P., Asensio, O.I., et al., 2003. Non-vacuum processing of $CuIn_{1-x}Ga_xSe_2$ solar cells on rigid and flexible substrates using nanoparticle precursor inks. Thin Solid Films 431–432, 53–57.

Kim, Y.C., Jeong, H.J., Lee, S.K., Kim, S.T., Jang, J.H., 2019. The effect of S/(S + Se) ratios on the formation of secondary phases in the band gap graded $Cu_2ZnSn(S, Se)_4$ thin film solar cells. J. Alloys Compd. 793, 289–294.

Kim, S.Y., Rana, T.R., Kim, J., Yang, K., Kang, J., Kim, D., 2018. Limiting effects of conduction band offset and defect states on high efficiency CZTSSe solar cell. Nano Energy 45, 75–83.

Neuwirth, M., Seydel, E., Seeger, J., Welle, A., Kalt, H., Hetterich, M., 2018. Band-gap tuning of $Cu_2ZnSn(S, Se)_4$ solar cell absorbers via defined incorporation of sulphur based on a post-sulphurization process. Sol. Energy Mater. Sol. Cells 182, 158–165.

Niu, G., Li, W.Z., Meng, F.Q., Wang, L.D., Dong, H.P., Qiu, Y., 2014. Study on stability of $CH_3NH_3PbI_3$ films and effect of post modification by Aluminum oxide in all-solid-state hybrid solar cells. J. Mater. Chem. A 2, 705–710.

Platzer-Bjorkman, C., Frisk, C., Larsen, J.K., Ericson, T., Li, S.Y., Scragg, J.J.S., Keller, J., Larsson, F., Torndahl, T., 2015. Reduced interface recombination in Cu_2ZnSnS_4 solar cells with atomic layer deposition $Zn_{1-x}Sn_xO_y$ buffer layers. Appl. Phys. Lett. 107, 243904.

Salomé, P.M.P., Malaquias, J., Fernandes, P.A., Ferreira, M.S., Cunha, A.F., Leitao, J.P., Gonzale, J.C., Matinaga, F.M., 2012. Growth and characterization of $Cu_2ZnSn(S, Se)_4$ thin films for solar cells. Sol. Energy Mater. Sol. Cells 101, 147–153.

Shin, D., Saparov, B., Mitzi, D.B., 2017. Defect engineering in multinary earth-abundant chalcogenide photovoltaic materials. Adv. Energy Mater. 7, 1602366.

Sun, K.W., Yan, C., Liu, F.Y., Huang, J.L., Zhou, F.Z., Stride, J.A., Green, M., Hao, X.J., 2016. Over 9% efficient Kesterite Cu_2ZnSnS_4 solar cell fabricated by using $Zn_{1-x}Cd_xS$ buffer layer. Adv. Energy Mater. 6, 1600046.

Tang, D., Wang, Q.L., Liu, F.Y., Zhao, L.B., Han, Z.L., Sun, K.W., Lai, Y.Q., Li, J., Liu, Y.X., 2013. An alternative route towards low-cost Cu_2ZnSnS_4 thin film solar cells. Surf. Coat. Technol. 232, 53–59.

Todorov, T.K., Reuter, K.B., Mitzi, D.B., 2010. High-efficiency solar cell with earth-abundant liquid-processed absorber. Adv. Mater. 22, 156–165.

Wanda, M.D., Ouédraogo, S., Ndjaka, J.M.B., 2019. Theoretical analysis of minority carrier lifetime and Cd-free buffer layers on the CZTS based solar cell performances. Optik 183, 284–293.

Wang, W.H., Cai, H.L., Chen, G.L., Chen, B.W., Yao, L.Q., Dong, J.B., Yu, X.X., Chen, S.Y., Huang, Z.G., 2018. Preparation of Sn loss-free Cu_2SnS_3 thin films by an oxide route for solar cell. J. Alloys Compd. 742, 860–867.

Wang, K.C., Hsu, H.R., Chen, H.S., 2017a. Study of surface sulfurization of $Cu_2ZnSn(S, Se)_4$ thin film solar cell by sequential H_2Se-selenization/H_2S-sulfurization. Sol. Energy Mater. Sol. Cells 163, 31–37.

Wang, W.H., Wang, G.H., Chen, G.L., Chen, S.Y., Huang, Z.G., 2017b. The effect of sulfur vapor pressure on Cu_2ZnSnS_4 thin film growth for solar cells. Sol. Energy 148, 12–16.

Wang, W., Winkler, M.T., Gunawan, O., Gokmen, T., Todorov, T.K., Zhu, Y., Mitzi, D.B., 2014. Device characteristics of CZTSSe thin-film solar cells with 12.6% efficiency. Adv. Energy Mater. 4, 1301465.

Washio, T., Shinji, T., Tajima, S., Fukano, T., Motohiro, T., Jimbo, K., Katagiri, H., 2012. 6% Efficiency Cu_2ZnSnS_4-based thin film solar cells using oxide precursors by open atmosphere type CVD. J. Mater. Chem. 22, 4021–4024.

Xu, J.X., Lin, J.H., Zhuang, C., 2018. Analysis of the open-circuit voltage of $Cu_2ZnSn(S, Se)_4$ thin film solar cell. Sol. Energy 164, 231–242.

Yang, K.J., Son, D.H., Sung, S.J., Sim, J.H., Kim, Y.I., Park, S.N., Jeon, D.H., Kim, J.S., Hwang, D.K., Jeon, C.W., Nam, D., Cheong, H., Kang, J.K., Kim, D.H., 2016. A band-gap-graded CZTSSe solar cell with 12.3% efficiency. J. Mater. Chem. A 4, 10151–10158.